UNIVERSITY OF CALIFORNIA SAN DIEGO

Characterizing the interaction between PTP4A1 and SRC

A thesis submitted in partial satisfaction of the requirements

for the degree Master of Science

in

Biology

by

Ruiyuan Zhang

Committee in charge:

Professor Nunzio Bottini, Chair
Professor Enfu Hui, Co-Chair
Professor Lifan Lu

2020

The thesis of Ruiyuan Zhang is approved, and it is acceptable in quality and form for publication on microfilm and electronically:

_____

_____
Co-chair

_____
Chair

University of California San Diego

2020

TABLE OF CONTENTS

ACKNOWLEDGEMENTS

The whole thesis is currently being prepared for submission for publication.

Chapter 5 contains unpublished experiments coauthored with Cristiano Sacchetti, PhD and Denise Beckmann, PhD from the Bottini Lab. The thesis author was the primary author of this chapter.

LIST OF ABBREVIATIONS

SSc: systemic sclerosis

RA: rheumatoid arthritis

SPR: surface plasmon resonance

PLA: proximity ligation assay

NMR: nuclear magnetic resonance

DF: dermal fibroblast

NHDF: normal human dermal fibroblast

SScDF: dermal fibroblasts from SSc patients

PFA: paraformaldehyde

ECM: extracellular matrix

TGFβ: transforming growth factor β

SMAD3: mothers against decapentaplegic homolog 3

αSMA: α-smooth muscle actin

PTP: protein tyrosine phosphatase

PTP4A1: protein tyrosine phosphatase IVA I, which is also known as Prl-1 for phosphatase of regenerating liver-1

CNNM2: magnesium transporters of the cyclin M2

CSK: C-terminal SRC kinase

TCPTP: T-cell protein tyrosine phosphatase

DUSP22: dual specificity phosphatase 22

DiFMUP: 6,8-Difluoro-4-Methylumbelliferyl Phosphate

pNPP: p-Nitrophenyl Phosphate

OMFP: 3-O-Methylfluorescein Phosphate

ASO: Anti-sense Oligonucelotide

BCA: Bicinchoninic Acid

LIST OF FIGURES

ABSTRACT OF THE THESIS

Characterizing the interaction between PTP4A1 and SRC

by

Ruiyuan Zhang

Master of Science in Biology

University of California San Diego, 2020

Professor Nunzio Bottini, Chair
Professor Enfu Hui, Co-Chair

It was previously shown by the Bottini Lab that PTP4A1 promotes TGFβ signaling and fibrosis in Systemic Sclerosis (SSc) via its interaction with SRC kinase (1). This thesis aims at further characterizing this interaction and looking for any factors potentially affecting it. Recombinant proteins were purified from *Escherichia coli*. Two *in vitro* co-precipitation assays were established and optimized to look at the interaction reliably and reproducibly, and the effect of various factors was examined with the assistance of the Surface Plasmon Resonance (SPR) assay. The characterization led us to propose an interaction mechanism between PTP4A1 and SRC which results in the enhancement of the pro-fibrotic signaling triggered by TGFβ. The relevance of the interaction was also confirmed in SSc dermal fibroblasts and mouse tissue using Proximity Ligation Assay (PLA) performed by other Bottini lab members. Together, these data

further demonstrate the critical role of the PTP4A1/SRC interaction in SSc and indicate that PTP4A1 might serve as a therapeutic target.

Introduction

Systemic Sclerosis (SSc) is a severe autoimmune disease characterized by progressive fibrosis of the skin and internal organs. The prevalence of the disease is around 20 cases per 100,000 US population, and it is highly lethal with serious complications, such as pulmonary arterial hypertension, heart failure and digital vasculopathy (2, 3). There is currently no cure for the disease itself, but regular screening and timely management of complications can substantially prolong patient survival (4). SSc cases can be further classified into limited cutaneous and diffuse cutaneous SSc based on the extent of skin involvement, with a small number (<5%) of SSc sine scleroderma cases. Although the classification provides some insights into the typical features of each subset, the manifestations differs significantly from patient to patient, suggesting the need for personalized treatment (5, 6). Besides, like many other autoimmune diseases, SSc incidence varies with gender, with approximately a 5:1 female to male ratio.

The cellular and molecular mechanism underlying the pathogenesis and progression of SSc is far from fully understood, but it involves dysregulation and crosstalk among vascular, immune and connective components, among which myofibroblasts are identified as the key effector cell type (3, 7). Endothelial damage and accumulation of ECM components activate both the innate and adaptive immune systems, leading to the secretion of several regulators that promote the differentiation of fibroblasts into myofibroblasts and the production of excessive ECM components (8, 9). Transforming growth factor β (TGFβ) is among the mediators secreted by immune cells like macrophages and is recognized as a key driver of pro-fibrotic pathways in fibroblasts (10). Upon binding to its receptor, TGFβ induces a signaling cascade through phosphorylation that results in nuclear translocation of mothers against decapentaplegic homolog

(SMAD), activating the production of α-smooth muscle actin (αSMA) and ECM proteins like collagen and fibronectin.

Protein Tyrosine Kinases (PTK) and Protein Tyrosine Phosphatases (PTP) are two families of mediators of cell signaling pathways that counteract each other's action by respectively phosphorylating and dephosphorylating their substrates. In contrast to PTKs, whose inhibitor Nintedanib has demonstrated alleviating effects in interstitial lung disease caused by SSc in a clinical trial last year (11), the role of PTPs in SSc remains largely unexplored, and so is their potential to serve as therapeutic targets. In a previous paper published by our lab (1), Protein Tyrosine Phosphatase IVA I (PTP4A1) was shown to be one of the PTPs whose expression is significantly higher in SSc patients compared to healthy subjects. On the contrary, PTP4A2, a close homolog of PTP4A1, did not demonstrate elevated expression. The study also found PTP4A1 to be a mediator within the TGFβ signaling pathway and a driver of the expression and nuclear translocation of SMAD3. It was observed to interact directly with SRC kinase and to promote its basal activity and half-life along the SRC-MEK-ERK-SMAD3 pathway.

PTP4A1 belongs to a family of PTPs composed of only PTP4A1, 2 and 3, which share high sequence similarity (13). Structurally, they share a PTP catalytic domain at the N-terminus, a polybasic region and a prenylation CAAX sequence at the C-terminus (14). As in many other PTPs, the phosphatase activity of PTP4A1-3 involves a catalytic cysteine (C104 in PTP4A1 and 3 and C101 in PTP4A2), but a notable characteristic of this family is the presence of a second conserved cysteine (C49 in PTP4A1 and 3 and C46 in PTP4A2) nearby in the three-dimensional structure that can form a disulfide bond with the catalytic cysteine to inactivate the enzymes under mildly oxidizing conditions. Functionally, no physiological substrate of PTP4A1 has been

identified and PTP4A1 showed exceptionally slow kinetics towards small molecule synthetic substrates including 6,8-Difluoro-4-Methylumbelliferyl Phosphate (DiFMUP), p-Nitrophenyl Phosphate (pNPP) and 3-O-Methylfluorescein Phosphate (OMFP) (17). The transcription factor ATF-7 and the magnesium transporters of the cyclin M2 (CNNM2) were reported to interact with PTP4A1 (18, 19). Members of the PTP4A family, especially PTP4A1 and PTP4A3, have recently attracted a lot of attention due to their overexpression in various cancer types, which correlates with metastasis and poor patient survival (21). Besides, PTP4A1 is also involved in liver regeneration and a recent study reported its role in synaptogenesis (22, 23).

As the first identified proto-oncogene, SRC kinase has been studied much more extensively in both its structure and function. It is a multidomain tyrosine kinase comprised of, from N- to C-terminus, an N-terminal tail, a SRC homology domain 3 (SH3), a SRC homology domain 2 (SH2), a catalytic domain and a short C-terminal regulatory tail. An important feature that has been well studied about SRC is the regulation of its kinase activity via phosphorylation of two important tyrosine residues, Y416 and Y527 (24, 25). Phosphorylation of Y527, catalyzed by C-terminal SRC kinase (CSK), recruits the SH2 and SH3 domains to the surface of the catalytic domain, which causes a rotation of α-helix C and ultimately the activation loop to block access to the active site (Figure 1, left). Many PTPs are hypothesized to dephosphorylate Y527 so that the SH2 and SH3 domains of SRC are freed to interact with specific substrates and the active site returns to function (Figure 1, center). In this form, phosphorylation of Y416 in the activation loop by another SRC molecule further enhances its kinase activity (Figure 1, right).

With the previous study setting an excellent basis, my research focuses on further characterizing the interaction between PTP4A1 and SRC. With the co-precipitation assays established to show direct and specific binding between PTP4A1 and SRC (Chapter 1), it is

found that oxidation of PTP4A1 promotes the interaction (Chapter 2). While phosphorylation on SRC Y416 does not show a significant effect, phosphorylation on Y527 decreases the interaction significantly (Chapter 3). The study about the SH3 and SH2 domains of SRC with the co-precipitation assays and Surface Plasmon Resonance (SPR) revealed that both domains are directly involved in the interaction (Chapter 4). The characterization led to a hypothesis in which the interaction occurs preferentially between oxidized PTP4A1 and the open form of SRC, which helps explain the overall basal SRC activity-enhancement observed previously as a result of the interaction.

Besides the in vitro assays using recombinant proteins, the PTP4A1/Src interaction was examined in NHDF and mouse tissue using Proximity Ligation Assay (PLA), which was performed by Cristiano Sacchetti and Denise Beckmann from our lab. It demonstrated enhanced interaction in NHDF after TGFβ stimulation and in fibrotic mouse tissue (Chapter 5). These data further show that the interaction between PTP4A1 and SRC is critical to pro-fibrotic signaling and SSc progression, and suggest that drugging PTP4A1 might yield beneficial clinical outcomes.

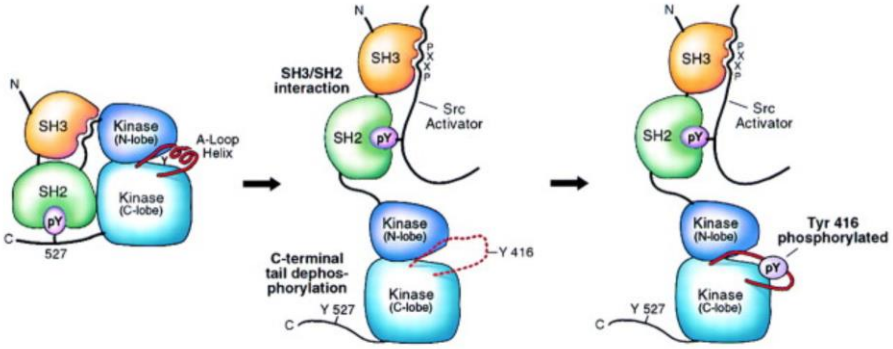

Figure 1. Schematic illustration of the effect of phosphorylation on Y416 and Y527 on the structure and activity of SRC (from ref. 25). Phosphorylation on Y527 is critical for the conversion between a closed and less active form of SRC and an open and active form of SRC. Phosphorylation on Y416 in the open form of SRC further promotes its activity.

Chapter 1

Development of two robust co-precipitation assays to study the association between SRC and PTP4A1

Methods:

Recombinant protein production and purification from E. coli.

Human PTP4A1 (residues 1-160) was subcloned into the NdeI/BamHI site of pET28a (Novagen) and expressed in *E. coli* BL21 (DE3) as an N-terminal 6-Histidine fusion. Bacterial cultures were grown at 37 °C and induced with isopropyl-1-thio-β-d-galactopyranoside (IPTG) at room temperature overnight. PTP4A1 was highly expressed and remained soluble after *E. coli* was lysed. It was purified by Ni-NTA affinity chromatography (Qiagen) and cation exchange chromatography (Biorad, 158-0040) at pH 7.3. For the co-precipitation assay using Ni-NTA (see below), the 6-Histidine tag was kept, and size exclusion chromatography (ENrich SEC 650, Bio-rad) was performed to ensure protein quality. For the co-precipitation assay using NHS activated agarose, the 6-Histidine tag was removed by thrombin digestion before the size exclusion chromatography step.

According to published data, SRC remains largely insoluble when expressed alone in *E. coli* and co-expression with *Yersinia* YopH phosphatase significantly increases its solubility (26). Thus, competent *E. coli* BL21 (DE3) transformed with YopH in pCDF-Duet (Novagen) was prepared using the $CaCl_2$ method. Full-length human SRC was subcloned in the BamHI/EcoRI site of pGEX-4T1 and co-expressed with YopH as an N-terminal GST fusion. Bacterial cultures were grown at 37 °C and induced with IPTG at 18 °C for 24 h. Both proteins were expressed and SRC remained partly soluble after cells were lysed. The soluble fraction was dialyzed overnight

to remove endogenous glutathione and SRC was purified by glutathione affinity chromatography (Sigma Aldrich, G4510). The GST tag was then removed by thrombin digestion, a second step of glutathione agarose and a size exclusion chromatography step.

All the cloning was confirmed by sequencing and the expression level and protein purity were assessed by SDS-PAGE.

In vitro co-precipitation assays

To prepare the PTP4A1 Ni-NTA Agarose beads for the co-precipitation assays, 0.1 mg PTP4A1 with intact N-terminal 6-Histidine tag in 1 mL of 150 mM NaCl and 20 mM Tris pH 7.3 was mixed with 100 µL Ni-NTA Agarose beads (Qiagen) at 4 °C overnight. The beads were then washed and resuspended in 1 mL buffer. The binding efficiency was analyzed by SDS-PAGE. To prepare Agarose beads covalently coupled to PTP4A1, 0.5 mg PTP4A1 in 1 mL DPBS was mixed with 75 mg dry NHS-activated Agarose beads at 4 °C overnight. After several washes, unreacted NHS groups were quenched with 1 mL 1 M ethanolamine, pH 8.2 at room temperature for 20 min. The beads were washed again and resuspended in 1 mL DPBS. The binding efficiency was analyzed by SDS-PAGE and the amount of protein on the beads was quantified using the Bicinchoninic Acid (BCA) assay (Thermo Scientific). In the co-precipitation assays, 0.5 µg SRC in 1 mL binding buffer (60 mM HEPES pH 7.4, 5 mM MgCl2, 5 mM MnCl2, 1% BSA) was combined with 20 µL beads suspension at 4 °C for 2 h. The beads were washed 3 times with the same buffer containing 50 mM imidazole and resuspended in 15 µL Laemmli buffer. The bound proteins were then analyzed by SDS-PAGE followed by western blotting and immunodetection. The mouse anti-PTP4A1/2 (clone 42) antibody was purchased from EMD Millipore (Billerica, MA). Mouse anti-SRC (clone L4A1) was purchased from Cell Signaling Technology (Danvers, MA).

Results:

In order to study the interaction between PTP4A1 and SRC in vitro, recombinant proteins were expressed and purified from *E. coli* (Figure 2). PTP4A1 was selected as the bead-bound bait and it showed efficient binding to both Ni-NTA Agarose and NHS-activated Agarose (Figure 1 A-B). Bare Ni beads and 5% BSA were utilized as negative controls. With the BCA assay showing good linearity when different amounts of NHS beads bound with protein were analyzed, it was used to quantify the protein concentration on the beads by comparing the readout from protein solution at known concentrations and bead samples (Figure 1 C). The calculated protein concentration was 0.129 ± 0.003 mg/mL beads for PTP4A1 and 0.147 ± 0.021 mg/mL beads for BSA, which are comparable.

In the co-precipitation assays, SRC bound directly and specifically to beads-bound PTP4A1 (Figure 2). Minimal amount of SRC was observed on the negative controls using either bare Ni beads or NHS bound with BSA.

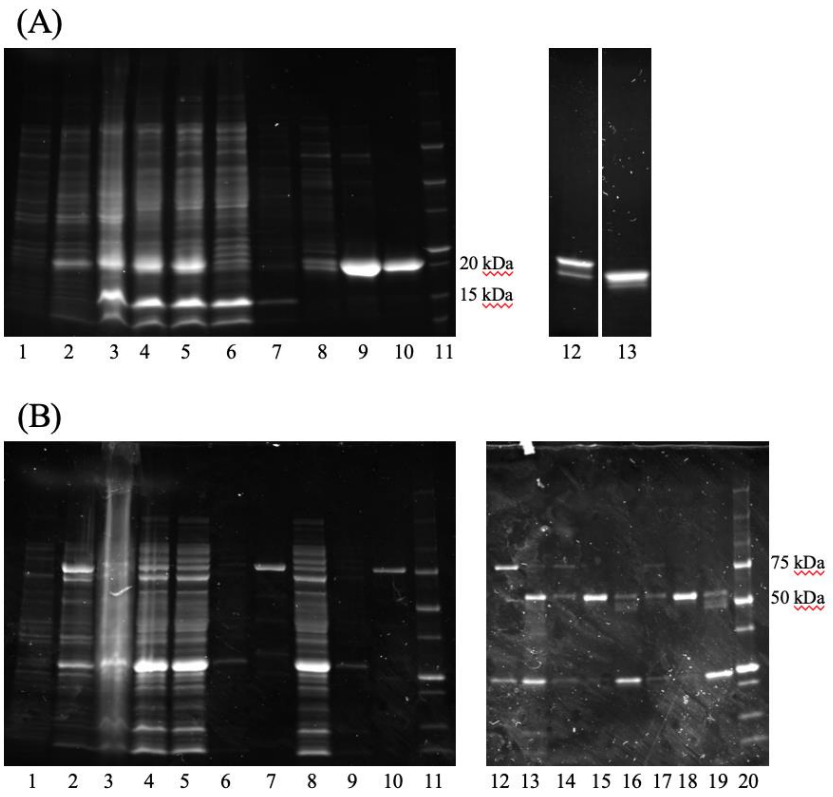

Figure 2. SDS-PAGE shows the purification of recombinant PTP4A1 and SRC. (A) Representative stain-free images of SDS-PAGE analysis (Biorad, catalog 17000928) of the purification of recombinant PTP4A1. Lanes 1-4 are samples from: 1) *E. coli* cultures before and 2) after induction, 3) *E. coli* lysates and 4) supernatants after DNAse treatment. Lanes 5-10 are samples from Ni-NTA affinity chromatography 5) load, 6) flowthrough, 7) wash and 8-10) 3 elutions. Lane 11 is Unstained Protein Standard (Biorad, catalog 1610363). Lane 12 is a sample from the elution from cation exchange chromatography and lane 13 is one from the elution from gel filtration chromatography after Thrombin was used to cleave the His-tag. (B) Representative images of stain-free SDS-PAGE analysis of the purification of recombinant SRC. Lane 1-4 are samples from: 1) *E. coli* cultures before and 2) after induction, 3) *E. coli* lysates and 4) supernatants after DNAse treatment. Lanes 5-10 are samples from glutathione agarose affinity chromatography: 5) flowthrough, 6) wash, 7) elution, and 8-10) flowthrough, wash and elution after reloading. Lanes 11 and lane 20 are Unstained Protein Standard. Lanes 12 and 13 are samples before and after thrombin cleavage of GST tag. Lanes 14-16 are samples from the second glutathione agarose affinity chromatography: 14) flowthrough, 15) wash and 16) elution. Lanes 17-19 are samples from gel filtration chromatography where lane 18 is the fraction containing SRC. Due to the presence of a native thrombin sensitive site in the N-terminal tail, the thrombin cleavage step was performed under controlled conditions (not shown).

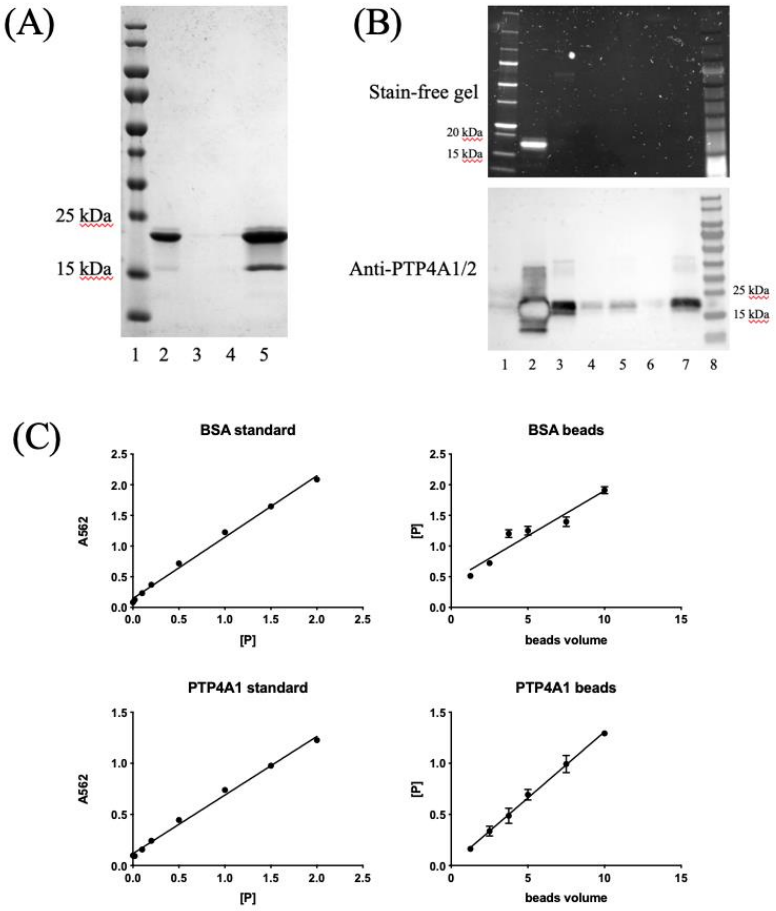

Figure 3. PTP4A1 binds efficiently to both Ni-NTA agarose and NHS-activated agarose. (A) SDS-PAGE stained with Coomassie shows that almost all His-tagged PTP4A1 from the input bound onto Ni-NTA Agarose. Lanes are: 1) PageRuler Prestained Protein Ladder (Thermo Scientific, catalog 26616), 2) protein input, 3) supernatant after binding, 4) washing after binding and 5) Ni-NTA bound with PTP4A1 respectively. (B) Stain-free SDS-PAGE and anti-PTP4A1/2 Western blot show that most PTP4A1 from the input bound onto NHS-activated agarose beads. Lanes are: 1) Unstained Protein Standard, 2) protein input, 3) supernatant after binding, 4) washing after binding, 5) supernatant after ethanolamine quenching, 6) washing after quenching, 7) NHS bound with PTP4A1 and 8) PageRuler Prestained Protein Ladder. (C) Plotted readout from the BCA assay. BSA and PTP4A1 were used as the standard of the beads respectively and plotted as absorbance at 562nm vs. protein amount (μg). The amount of proteins bound on the beads was calculated using the equation derived from the standard and plotted against the volume of beads applied (μL). Triplicate assays were performed on each sample and the data are presented as mean ± SD.

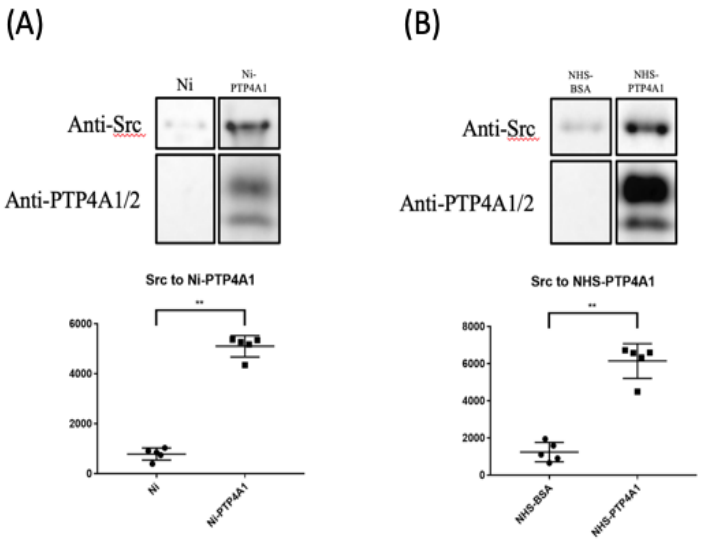

Figure 4. In vitro co-precipitation assays demonstrate specific binding of purified SRC to PTP4A1.
(A) Representative Western Blot image along with a graph of the corresponding densitometric analysis (n=5) showing specific binding of purified full-length SRC to Ni-NTA Agarose-bound 6×His-tagged PTP4A1. Bare Ni-NTA beads were used as a negative control. Data are presented as mean ± SD. Statistical significance was assessed using the Mann-Whitney test, **P<0.01. (B) Representative Western Blot image along with a graph of the corresponding densitometric analysis (n=5) showing specific binding of purified full-length SRC to PTP4A1 covalently attached to NHS-activated Agarose. NHS-activated Agarose-bound BSA was used as a negative control. Data are presented as mean ± SD. Statistical significance was assessed using the Mann-Whitney test, **P<0.01.

Discussion:

This chapter describes how two co-precipitation assays were established to show the direct and specific binding of SRC to PTP4A1 in their purified forms. In other words, the interaction can occur without the mediation of other proteins or factors. The difference between the binding of SRC to the beads bound with PTP4A1 and negative control is clear enough for the assays to be used to study how different factors might affect the interaction. Moreover, the two beads systems provide alternatives that can be used in different situations in which, due to the properties of the linkage between PTP4A1 and the beads, one may work better than the other. For example, Ni-NTA agarose is more suitable than NHS-activated agarose for assays where the oxidation state of PTP4A1 is studied.

The PTP4A1 band observed in NHS-activated agarose bound with PTP4A1 was a little surprising since the linkage between the protein and the beads is supposed to be covalent. Possible explanations for this include the breaking of the covalent bond by the Laemmli buffer used in SDS-PAGE and the formation of the multimers of PTP4A1 on the beads. The latter has been observed by other research groups in the crystal structures and cellular assays (16, 17). Since trimerization was suggested to localize PTP4A1 near the plasma membrane which is also where SRC is usually found in fibroblasts, it might affect, and presumably enhance, the interaction (39). A pitfall is that the conditions used for the in vitro assays might not reflect the cellular environment perfectly, which is always a concern in assays using purified proteins. The presence of other proteins and factors inside the cell might significantly influence the interaction between PTP4A1 and SRC.

Chapter 2

Effect of the oxidation state of PTP4A1 on the interaction

Methods:

The oxidation and reduction of PTP4A1 on Ni-NTA Agarose

20 µL Ni-NTA beads bound with PTP4A1 were incubated in 150 mM NaCl, 20 mM Tris, pH 7.3 with either 0.5 mM H_2O_2 or 20 mM DTT for 1 h at 4 °C. The buffer was removed before the co-precipitation with SRC which was conducted as described in chapter 1. The only difference is that the final bead samples were resuspended in 15 µL non-reducing Laemmli buffer to preserve the oxidation states of PTP4A1 for later analysis.

Results:

As mentioned in the introduction, the activity and local conformation of PTP4A1 can be regulated by its oxidation, which leads to formation of a disulfide bond between the catalytic C104 and nearby C49. In this chapter, how the oxidation states of PTP4A1 might affect its interaction with SRC was examined. The co-precipitation assay with the Ni-NTA system was chosen over the NHS system since PTP4A1 bound to beads could be eluted easily and analyzed for its oxidation state. As seen in the anti-PTP4A1/2 blot of Figure 5, H_2O_2 and DTT oxidized and reduced most of the protein on the beads respectively and the negative control yielded an intermediate state. Figure 5 shows a representative western blot image using an anti-SRC primary antibody (upper panel) and the quantification of 3 independent replicates (lower panel) indicating that more SRC was associated with oxidized PTP4A1 and the amount decreased with increasing levels of reduced PTP4A1. The results suggest that the oxidation of PTP4A1 promotes its interaction with SRC.

Oxidizing or reducing PTP4A1 on NHS-activated agarose was also attempted using the same protocol. However, for unknown reasons, only a decrease in the reduced band, but not an increase in the oxidized band, was seen when H_2O_2 was used (data not shown). In the future we plan to experiment with an alternative protocol where the protein is oxidized or reduced before binding to the beads.

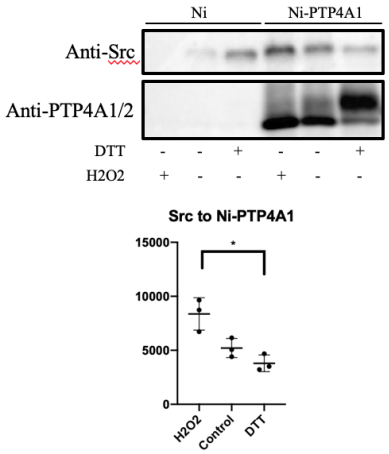

Figure 5. In vitro co-precipitation assay demonstrates that oxidation of PTP4A1 promotes its interaction with SRC. Representative Western blot image along with a graph of the corresponding densitometric analysis (n=3) showing that the oxidation of PTP4A1 promotes the binding to SRC. Data are presented as mean ± SD. Statistical significance was assessed using the one-way ANOVA test, *P<0.05.

Discussion:

This chapter shows that the oxidation of PTP4A1 strengthens its interaction with SRC in the co-precipitation assay using the Ni-NTA system. Since oxidation only drives localized conformational changes on PTP4A1 near its active site, our study greatly narrows down the potential critical residues contributing to the interaction (17). In addition, the observation is consistent with the known pathogenic role of oxidation in fibrosis and SSc. The importance of oxidative stress in the pathogenesis and progression of SSc was proposed by Murrel as early as 1993 (27). Later studies demonstrated that a higher level of reactive oxidizing species (ROS) was detected in SSc patient skin samples as well as sorted cells including fibroblasts. Moreover, the application of antioxidants like vitamin E showed some beneficial effects in clinical trials (28). Pathologically, ROS could alter the fibrotic pathways in various ways including modifying the oxidation state of intracellular proteins. So, it is reasonable to hypothesize that the highly oxidative environment of fibrotic tissues tends to convert PTP4A1 -whose expression is enhanced by TGFβ in the same tissues- to its oxidized form in fibroblasts, promoting its interaction with SRC. In a positive pro-fibrotic feedback, this interaction can then further enhance the signaling transferred along the MAPK pathways and result in the nuclear localization of SMAD3 and the expression of pro-fibrotic genes. The hypothesis could be tested in NHDF by co-incubation with H_2O_2 with or without TGFβ. However, treatment with H_2O_2 could induce a variety of effects intracellularly and it might be difficult to sort out effects specifically due to PTP4A1. In addition, Cys oxidation was shown to also decrease the interaction between PTP4A phosphatases and CNNM which could further complicate data interpretation (29). Interestingly, in a previous study PTP4A1 carrying mutations of Cys in the C-terminus (PTP4A1 C170S C171S) was found to be much more reduced when it was purified

from *E. coli* compared to PTP4A1 wt (30) suggesting that the C-terminus of PTP4A1, might regulate the oxidation and reduction of the enzyme. Another potential avenue for future investigation is whether the oxidation of PTP4A1 affects its ability to trimerize.

Chapter 3

Effect of SRC phosphorylation on Y416 and Y527 on the interaction

Methods:

Recombinant protein production and purification from E. coli.

Site-directed mutagenesis was performed to generate SRC Y527F and K295A. The two constructs were co-expressed with YopH and purified following the same protocol of SRC wt described in Chapter 1. CSK (residues 1-443) was subcloned into pET28a (Novagen) and expressed as a C-terminal 6-Histidine fusion. Bacterial cultures were grown at 37 °C and induced with isopropyl-1-thio-β-d-galactopyranoside (IPTG) at 18 °C for 16 h. CSK was highly expressed and remained soluble after *E. coli* was lysed. It was purified by Ni-NTA affinity chromatography (Qiagen) and size exclusion chromatography (ENrich SEC 650, Bio-rad). All the plasmid constructs and mutations were confirmed by DNA sequencing, and protein purity was assessed by SDS-PAGE.

Production of PTPs from E. coli and in vitro dephosphorylation assay

YopH was subcloned into pCDF-Duet (Novagen) and expressed as an N-terminal 6-Histidine fusion. CD45 and T-cell protein tyrosine phosphatase (TCPTP) were subcloned into pET28a (Novagen) respectively and expressed as N-terminal 6-Histidine fusions. Dual specificity phosphatase 22 (DUSP22) was subcloned into pGEX-4T1 and expressed as an N-terminal GST fusion. The 6-Histidine fused PTPs were purified with Ni-NTA affinity chromatography. The GST fused PTP was purified with Glutathione agarose affinity chromatography. The elutions from the affinity chromatography went through a size exclusion chromatography step for further purification. All the plasmid constructs were confirmed by DNA sequencing, and protein purity was assessed by SDS-PAGE.

After SRC wt was phosphorylated with CSK, ATP was removed by buffer exchange using a 10,000 MWCO protein concentrator (Sartorius) and an in vitro dephosphorylation assays were performed in 300 mM NaCl, 20 mM Tris, pH 8, 10 mM DTT at 30 °C up to 1h. Various concentrations of each PTP were tested.

In vitro phosphorylation assay

SRC selectively phosphorylated on Y416 or Y527 was obtained by autophosphorylation and phosphorylation by CSK respectively. SRC autophosphorylation was carried out with 0.05 mg/mL SRC wt or SRC Y527F in 300 mM NaCl, 20 mM Tris, pH 8, 10 mM MgCl2, 10 mM DTT, 1 mM ATP incubated at 30 °C. The mixture was sampled at specified time points to follow the course of the reaction by SDS-PAGE (see below). CSK-mediated phosphorylation of SRC was similarly studied with 0.05 mg/mL SRC K295A, 0.025mg/mL His-tagged CSK in the same buffer and condition. To maximize Y527 phosphorylation levels of SRC K295A, 0.2 mg/mL SRC K295A, 0.1 mg/mL His-tagged CSK in the same buffer were incubated at room temperature up to 16 h. The level of phosphorylation was assessed with either immunoblotting or phos-tag SDS-PAGE. For immunoblotting, rabbit anti-pSRC (Y416, catalog number 2101), rabbit anti-pSRC (Y527, catalog number 2105) were purchased from Cell Signaling Technology (Danvers, MA). Phos-tag gels were prepared with 10% acrylamide (Bio-rad, 1610158) with 0.35 M Bis-Tris, pH 6.8, 100uM ZnCl2, 50uM phos binding reagent (Apexbio Technology, NC1418011) and stained with InstantBlue (Expedeon, ISB1L).

In vitro co-precipitation assays

A volume of phosphorylation reaction including 0.5 μg SRC was utilized in the co-precipitation assay using the NHS-activated agarose system. For the assessment of the effect of phosphorylation on Y416, SRC Y527F was autophosphorylated for 5 min using the protocol

described above. For the assessment of the effect of phosphorylation on Y527, SRC K295A was phosphorylated with CSK for 16 h using the protocol described above. SRC mutants incubated in the same conditions but without addition of ATP were used as the negative controls. The procedure for the co-precipitation assays was the same as described in Chapter 1.

Results:

As mentioned in the introduction, the phosphorylation of SRC on Y416 and Y527 closely regulates the structure and activity of the enzyme in opposite directions: phosphorylation on Y416 has activating while phosphorylation on Y527 has inhibiting effects. In this chapter, whether each might affect the interaction between PTP4A1 and SRC was explored. In vitro autophosphorylation of purified SRC wt was conducted at first, and the Western blots showed that SRC wt can autophosphorylate on both Y416 and Y527, though the former appears to have a faster kinetic than the latter (Figure 6A). In order to focus the study on a single tyrosine residue at a time, several PTPs including YopH, CD45, TCPTP and DUSP22 were purified from *E. coli* and incubated with SRC after CSK phosphorylation to test whether any of them enabled dephosphorylation *in vitro* with enough specificity for one phospohotyrosine residue or the other to yield sufficient amounts of protein that could be used in the assays. Unfortunately, YopH, CD45 and TCPTP demonstrated equal ability to dephosphorylate SRC Y416 and Y527 while DUSP22 purified from *E. coli* was unable to dephosphorylate either (data not shown).

Thus, we approached the problem utilizing mutants of SRC that enable SRC phosphorylation on a single residue at a time. To study the effect of Y416 phosphorylation on the interaction, a SRC Y527F mutant was constructed and purified from *E. coli*. The mutant showed comparable autophosphorylation on Y416 as SRC wt in the *in vitro* phosphorylation assay

(Figure 6B). Allowing the autophosphorylation reaction to proceed for 5 min before the sample was used for the co-precipitation assay was sufficient to achieve nearly complete pY416 phosphorylation while minimizing autophosphorylation at minor sites such as Y213 and Y138 (36). Next, to ensure that the mutation itself does not affect SRC interaction with PTP4A1, a preliminary co-precipitation assay was performed and showed that without any phosphorylation, comparable amounts of SRC wt and Y527F mutant bind to PTP4A1 beads (Figure 6D). On that basis, unphosphorylated and autophosphorylated samples of SRC Y527F were applied to the co-precipitation assay with the NHS system. It was demonstrated that similar amount of SRC from the two samples binds to PTP4A1 in the anti-SRC western blot and the quantification (Figure 7A). The similar level of phosphorylation detected by anti-Y416-phosphorylated SRC antibody on the input and the PTP4A1 beads further indicated that Y416 phosphorylation does not affect binding.

To study the effect of the selective phosphorylation on SRC Y527 on the interaction, a kinase dead SRC mutant, SRC K295A was constructed. K295 is an essential residue for SRC to bind ATP and its mutation has been well established to impair kinase activity (31-33). SRC K295A was preferred over SRC Y416F because Y416F might retain some kinase activity and the mutation might affect the conformation and docking of the activation loop onto other surfaces in the SRC structure, which controls the accessibility of the active site. Since the active site of SRC is more deeply buried compared to the activation loop, there is less concern that the K295A mutation would alter the surface structure of SRC. Our in vitro phosphorylation assay clearly showed that CSK could specifically phosphorylate SRC K295A on Y527 (Figure 6C). Again, a preliminary co-precipitation assay was performed to show that the mutation itself and the addition of CSK do not affect SRC interaction with PTP4A1 (Figure 6D). Then, co-precipitation

assays were performed using the NHS system since His-tagged CSK present in the phosphorylation sample might cause non-specific binding in the Ni-NTA system. The assay was first attempted after a phosphorylation reaction with diluted SRC K295A and CSK at 30 °C for 5 min as described for the Y416 phosphorylation. In these assays we observed that the intensity of the anti-SRC bands precipitated by PTP4A1 beads was similar with or without phosphorylation, but SRC phosphorylation was hardly detected by anti-Y527-phosphorylated SRC antibody on precipitated SRC compared to the input (Figure 8A). This suggested that the phosphorylation on tyrosine 527 might inhibit SRC interaction with PTP4A1 and the lack of change in precipitated SRC amounts in the anti-SRC western blot could be due to low stoichiometry of SRC Y527 phosphorylation in the input. Thus, we subsequently optimized the phosphorylation reaction and a phos-tag gel-based approach was adopted to visualize the stoichiometry of phosphorylation. When a much higher concentration of SRC K295A and CSK was used, a clear band shift was observed on the phos-tag gel from 15 min, which is very likely to correspond to single and complete phosphorylation on Y527 (Figure 8B). The co-precipitation assay was repeated with the samples generated from the new protocol and in these experiments the intensity of the anti-SRC bands precipitated by PTP4A1 beads was significantly lower after phosphorylation. To conclude, the phosphorylation on Y527 decreases the interaction between SRC and PTP4A1, which suggests that the closed form of SRC interacts with PTP4A1 more weakly.

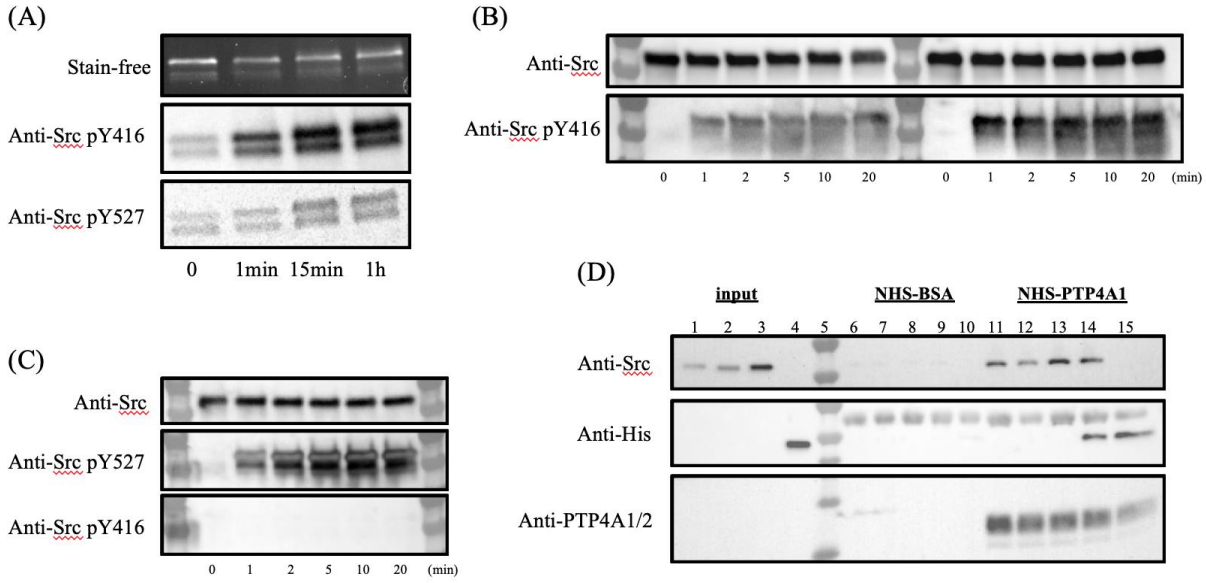

Figure 6. In vitro phosphorylation assays and an in vitro co-precipitation assay performed on SRC wt and mutants. (A) Representative Stain-free gel and Western Blot images of samples taken at different time points from SRC wt autophosphorylation. (B) Representative Western Blot images of samples taken at different time points from SRC wt and SRC Y527F autophosphorylation. (C) Representative Western Blot images of samples taken at different time points from CSK phosphorylation on SRC K295A. (D) Representative Western Blot images of co-precipitation assays using the NHS system on SRC wt, SRC mutants and CSK. SRC wt was applied to lanes 1, 6, 11; SRC Y527F to lanes 2, 7, 12; SRC K295A to lanes 3, 8, 13; SRC K295A and CSK in a 2:1 ratio to lanes 9 and 14; CSK alone to lanes 4, 10, 15. Anti-His antibody was used to detect CSK.

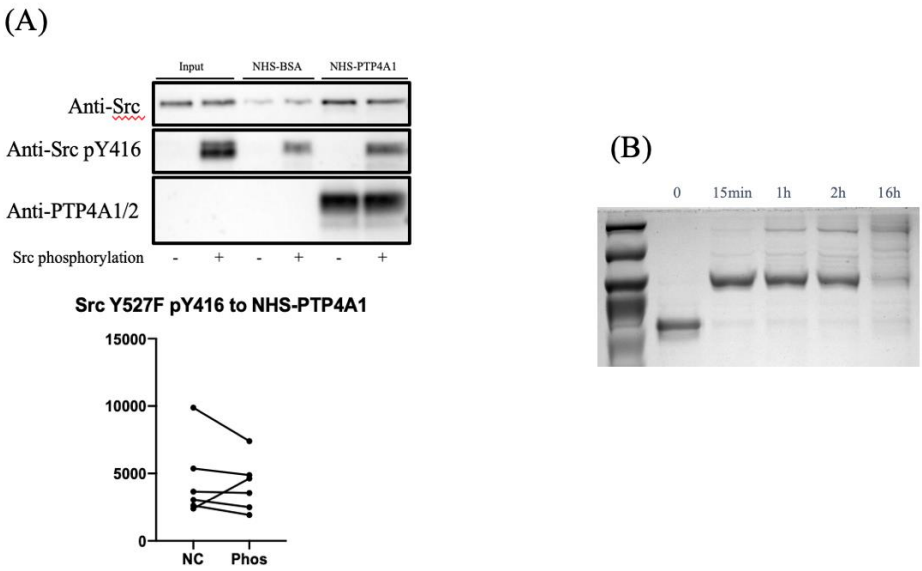

Figure 7. In vitro co-precipitation assays demonstrate that phosphorylation of SRC on Y416 does not affect the binding to PTP4A1. (A) Representative Western Blot image along with a graph of the corresponding densitometric analysis (n=6) showing that phosphorylation of Y416 using a SRC Y527F mutant has no measurable effect on its binding to PTP4A1 covalently attached to NHS-activated Agarose. Data are presented as mean ± SD. Statistical significance was assessed using the Mann-Whitney test. (B) Representative phos-tag gel image on samples taken at different time points from SRC Y527F autophosphorylation. The phosphorylation was performed with 0.2 mg/mL SRC Y527F in in 300 mM NaCl, 20 mM Tris, pH 8, 10 mM MgCl2, 10 mM DTT, 1 mM ATP incubated at room temperature.

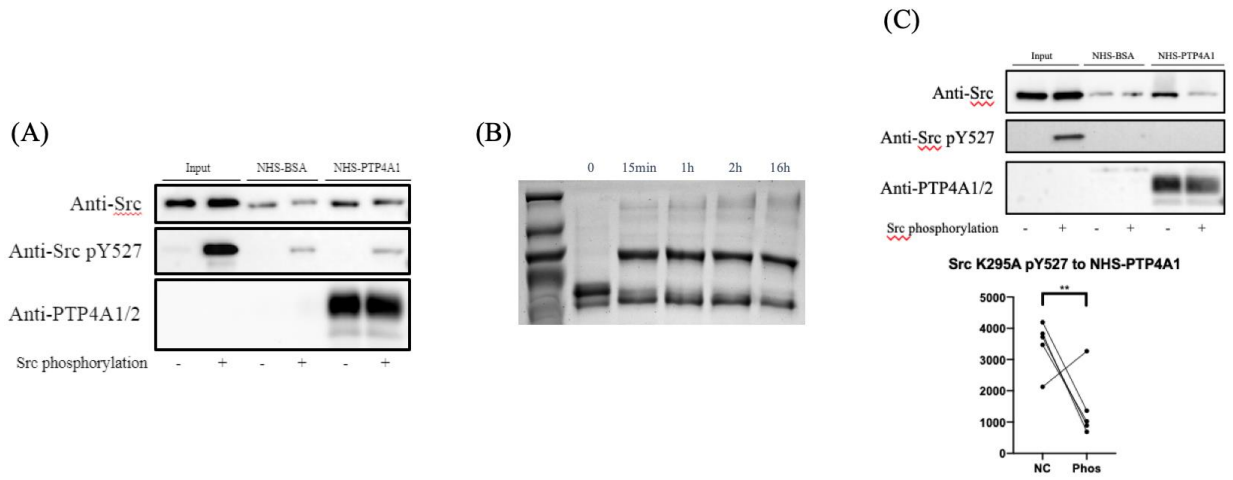

Figure 8. In vitro co-precipitation assays demonstrate that phosphorylation of SRC on Y527 suppresses binding to PTP4A1. (A) Representative Western blot image shows no significant change in SRC binding to PTP4A1 beads after phosphorylation, but the very weak signal detected by the anti-pY527 SRC co-precipitated with PTP4A1 suggests low stoichiometry of phosphorylation in the input and the phosphorylation might actually decrease the binding. (B) Representative phos-tag gel image of samples taken at different time points from the CSK phosphorylation reaction of SRC K295A using the optimized phosphorylation protocol. (C) Representative Western Blot image along with a graph of the corresponding densitometric analysis (n=5) showing that phosphorylation of Y527 using a SRC K295A mutant inhibits its binding to PTP4A1 covalently attached to NHS-activated Agarose. Data are presented as mean ± SD. Statistical significance was assessed using the Mann-Whitney test, **P<0.01.

Discussion:

This chapter shows distinct effects of the phosphorylation of SRC on Y416 and Y527 on its interaction with PTP4A1: phosphorylation on Y416 barely has any effect on the binding while that on Y527 significantly decreases it. Overall, this suggests that PTP4A1 preferentially interacts with the open vs. the closed form of SRC, regardless of phosphorylation on Y416. It further implies that the critical residues on SRC that interact with PTP4A1 might be near the interface between the catalytic domain and the combined SH3 + SH2 domains or at a location with significant structural change between the open and closed form of SRC.

In the previous study from our lab, knocking down PTP4A1 in NHDF using Anti-sense Olgonucleotides (ASO) resulted in decreased SRC protein level, an increase in both phosphorylation on Y416 and Y527, and a decrease in SRC activity substantiated by lower phosphorylation on PLCγ Y783, a specific target of SRC. Earlier publications have reported an inverse relationship between SRC activity and its stability, and the degradation of SRC is mediated by ubiquitination (34-35). A model was proposed where PTP4A1 interacts with SRC and enhances its basal activity to balance SRC protein level and kinetic activity. This would be achieved on one hand through inhibition of SRC phosphorylation on Y527 so that SRC remains in its open and active form, on the other hand PTP4A1 also would inhibit auto- or trans-phosphorylation on Y416 in order to moderate SRC degradation rates due to basal autoactivation. Our observation that the form of SRC that is highly phosphorylated on Y527, which tends to be in a closed, thus inactive conformation, has less affinity for PTP4A1 is highly consistent with this model. The end result is that PTP4A1 stabilizes SRC in an active form with less phosphorylation on Y527, to keep SRC basal activity within an optimal range and balance activity-dependent protein stability with the need to keep sufficient amounts of SRC in a

"poised" state needed to enable potential acute signaling events. What is left currently unexplained by our model is how PTP4A1 inhibits SRC phosphorylation on Y527 and also further work is needed to clarify the mechanism through which PTP4A1 inhibits SRC auto-phosphorylation on Y416. It is worth noticing that CSK alone in the preliminary co-precipitation assay showed specific binding to PTP4A1 (Figure 4D), which might suggest PTP4A1 could affect SRC phosphorylation on Y527 through CSK-mediated pathways. As for the mechanism through which PTP4A1 decreases SRC autophosphorylation in vitro, E6AP, an E3 ligase, has been suggested to interact with SRC directly and to catalyze its ubiquitination (34). Thus, it is possible that impairment of the binding of E6AP to SRC due to the interaction between SRC and PTP4A1 contributes to the stabilization of SRC.

Chapter 4

The contribution of SRC domains to the interaction

Methods:

Recombinant protein production and purification from E. coli.

Sequences encoding SRC SH3 (residues 81-142), SH2 (residues 148-245), and SH3 + SH2 (residues 81-248) were PCR amplified, cloned, expressed and purified following the same procedures as SRC except that no co-expression with YopH phosphatase was performed and the GST tag was not removed during the purification. Since aggregation was observed with SRC SH2 domain, 10 mM DTT was added to the buffer used for the size exclusion chromatography and the storage of the protein. All the cloning was confirmed by sequencing and the expression level and protein purity were assessed by SDS-PAGE.

In vitro co-precipitation assays

86 nmol of each domain was used for the co-precipitation assay with both the Ni-NTA system and the NHS system. GST alone was used as a negative control and the procedure for the assay was the same as described in Chapter 1.

Surface Plasmon Resonance (SPR) assay

PTP4A1 full length, PTP4A1 residue 1-169 and PTP4A2 full length were covalently immobilized onto the three channels of a CM5 chip. SRC combined SH3 + SH2 domains with N-terminal 6-Histidine tag generated by a collaborator was prepared at various concentrations (25 nM, 50 nM, 100 nM, 200 nM, 400 nM) with HBP-EP+ buffer (GE Healthcare). A titration with low to high concentrations was performed with the flow rate set to 30 μL/min. The association period was set for 180 sec. and the dissociation period for 900 sec.

Results:

As mentioned in the introduction, SRC SH3 and SH2 are highly involved in the regulation of the structure and activity, and of the interaction of SRC with other proteins. Whether they participate in the interaction between SRC and PTP4A1 is assessed in this chapter. Due to the lack of commercially available antibodies able to detect untagged SRC domains, the domains (SH3, SH2, and combined SH3 + SH2 domains) were expressed and purified with a N terminal GST tag. As shown in Figure 7, GST-tagged SH2 domain shows direct and specific binding to PTP4A1 while GST alone as a negative control barely binds in the co-precipitation assays. GST-tagged SH3 domain, on the other hand, did not show specific binding to PTP4A1 (Data not shown). In collaboration with another laboratory, a surface plasmon resonance (SPR) assay was performed with an NHS-activated chip bound with PTP4A1 full length, PTP4A1 1-169, and PTP4A2 full length. PTP4A1 1-169 is the shortened version of PTP4A1 lacking the prenylation site, which is associated with higher stability and yield from *E. coli*. It can be seen that His-tagged combined SRC SH3 + SH2 domain supplied in the flow bound to all three constructs of PTP4A1 and 2 (Figure 8A, 8B). Based on the dissociation constant (K_D) calculated from the binding curves, the domain displayed significantly higher affinity to PTP4A1 than to PTP4A2 while the affinity was similar between the shortened version of PTP4A1 and full-length PTP4A1 (Figure 8B, 8C). In conclusion, our data suggest that the SRC SH3 and SH2 domains contribute directly to the interaction between SRC and PTP4A1.

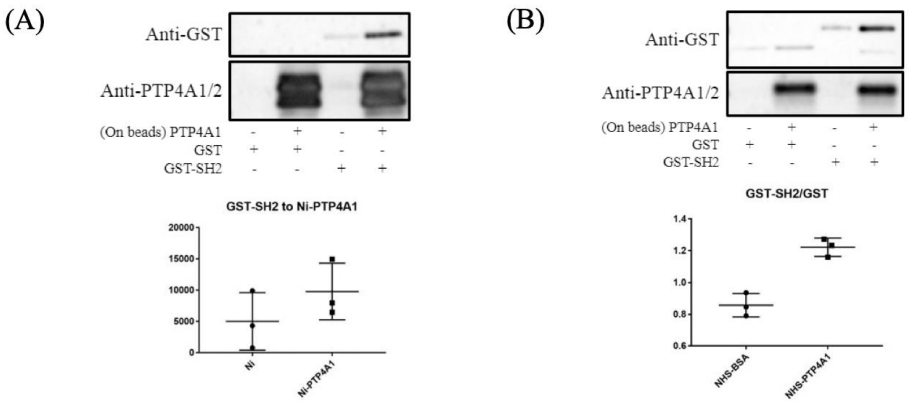

Figure 9. SRC SH2 domain alone specifically binds PTP4A1 in in vitro co-precipitation assays. (A) Representative Western Blot image along with a graph of the corresponding densitometric analysis (n=3) showing specific binding of purified SRC SH2 domain fused to N-terminal GST to Ni-NTA Agarose-bound 6×His-tagged PTP4A1. Data are presented as mean ± SD. The Mann-Whitney test so far does not show a significant difference, but it should be improved with more repeats. Paired t test generated a P value of 0.0154. (B) Representative Western Blot image along with a graph of the corresponding densitometric analysis (n=3) showing specific binding of purified SRC SH2 domain fused to N-terminal GST to PTP4A1 covalently bound to NHS-activated Agarose. Data are presented as mean ± SD of the ratio of GST-tagged SRC SH2 to GST alone on each beads type. The Mann-Whitney test so far does not show significant difference, but it should be improved with more repeats. Paired t test generated a P value of 0.0253.

(A)

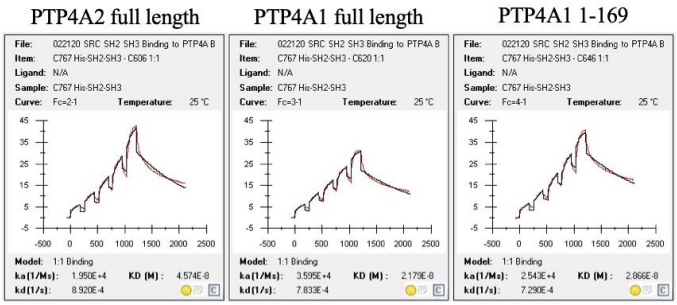

(B)

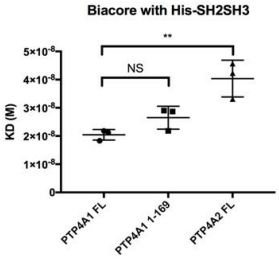

(C)

	PTP4A1 FL	PTP4A1 1-169	PTP4A2 FL
K_D (nM)	20.4 ± 1.87	26.5 ± 4.07	40.4 ± 6.52

Figure 10. Combined SRC SH3 + SH2 domains specifically bind PTP4A1 in Surface Plasmon Resonance (SPR) assay. (A) The red line represents the binding curves of His-tagged combined SRC-SH3 + SH2 onto immobilized PTP4A2 full length, PTP4A1 full length and PTP4A1 residues 1-169. The black line is generated theoretically from the 1:1 binding model. (B), (C) Graph and Table summarizing the dissociation constants (K_D) measured by the SPR (n=3) indicates that His-tagged combined SH3 + SH2 domains show higher affinity to PTP4A1 than to PTP4A2. Data presented as mean ± SD and statistical significance was assessed using one-way ANOVA, **P<0.01.

Discussion:

This chapter shows that both SRC SH2 and SH3 domains bind directly and specifically to PTP4A1. The affinity of SRC SH2 is higher than that of SH3 domain, and the affinity of the combined SH3 + SH2 domains is higher for PTP4A1 than to PTP4A2. These data are consistent with the idea, drawn from examining the effect of SRC phosphorylation, that PTP4A1 binds more strongly with the open form of SRC in which both SH3 and SH2 domains are released from the catalytic domain. The data also suggest that PTP4A1 might associate with residues on the two domains that are hidden in the closed form of SRC, resulting in the stabilization of the more active form of SRC. The identification of the exact residues involved in the direct interaction between SRC SH2, SH3 domains and PTP4A1 will require structural analyses such as co-crystallization or nuclear magnetic resonance (NMR). While crystals of PTP4A1 alone could be grown in high ammonium sulfate (1.5-2M) at a pH lower than neutral (acetate, pH 4.5 or 5.1), the co-crystallization with PTP4A1 and SRC SH3 + SH2 domains has not worked in our hands under the same conditions or other conditions included in common crystal screens. The NMR assignments of PTP4A1 residues have been published (37) and could be used here to identify the exact residues on PTP4A1 that mediate the interaction with SRC SH3 + SH2 domains. It might also be possible to get NMR assignments for the SRC SH3 + SH2 domains, since their MW is only around 20kDa, then leverage NMR to identify the SRC residues that mediate the association with PTP4A1.

It is worth noticing that the affinity of combined SH3 + SH2 domains to PTP4A1 is significantly higher than to PTP4A2. This might help to partly explain why knocking down PTP4A2 in NHDF did not affect SRC signaling in the previous study from our lab. However, since combined SH3 + SH2 domains still show a certain level of affinity to PTP4A2, some other

regulators are probably involved in complex formation and responsible for the fact that SRC is only interacting with PTP4A1 but not with PTP4A2 in NHDF.

A pitfall of our experiments is that the K_Ds calculated from the SPR binding curves might overestimate the binding affinity between SRC SH3 + SH2 domains and PTP4A1. A thermal shift assay was performed previously on PTP4A1 and isolated SRC domains and it demonstrated two individual melting temperatures though different protein concentrations and ratios were tested. In contrast, when PTP4A1 and CNNM2 were combined in the same assay, it resulted in a single melting temperature intermediate between the ones of the individual proteins, implying the formation of a high-affinity complex (not shown). Thus, conducting a titration by NMR might be a good option to verify the binding affinity between SRC domains and PTP4A1.

Chapter 5

PLA assay demonstrating the interaction in fibroblasts and mouse tissue

Methods:

Proximity Ligation Assay (PLA) and immunofluorescence staining of fibroblasts

The assay was performed according to the manufacturer's protocol (Sigma Aldrich). Briefly, NHDF or dermal fibroblasts from SSc patients (SScDF) were seeded on sterile coverslips in FBS-supplemented DMEM until 80% confluence and stimulated with TGFβ for 6 h. After washes with PBS, the cells were fixed with 4% paraformaldehyde (PFA), pH 7.4 for 20 min and permeabilized with 0.2% Tween-20 for 5 min. The cells were incubated in blocking solution containing 10% normal horse serum (NHS) for 1 h and then with mouse anti-PTP4A1/2 antibody 1:50 (EMD Millipore, clone 42, 05-1583) and rabbit anti-SRC antibody 1:100 (Cell Signaling, 2108S) at 4 °C overnight. Oligonucleotide-conjugated anti-mouse minus and anti-rabbit plus PLA secondary probes were added at appropriate dilutions prepared in PBS with 3% NHS and the cells were incubated in a humidified chamber for 1 h at 37 °C. The connector oligonucleotides were hybridized and circularized by ligation for 30 min at 37 °C. After thorough washing, the cells were incubated with DNA polymerase for 100 min at 37 °C to produce rolling circle amplification products tagged with a red fluorescence probe. The nuclei were counterstained with Hoechst 1:1000 (Sigma Aldrich) for 10 min, and the PLA signals were visualized at 60 x magnifications under Zeiss Confocal Microscope 780 and analyzed using the Zeiss software.

Mice

For the bleomycin-induced fibrosis model, 8–12-week-old female mice received seven subcutaneous injections every other day of 50 μg bleomycin sulfate dissolved in 100 μl

phosphate-buffered saline (PBS). Skin was dissected in the injection area, fixed in 10% Zinc Formalin for 24 h and processed and embedded in paraffin.

Results:

To demonstrate that the interaction between PTP4A1 and SRC is relevant in a cellular environment and the in fibrotic skin sections of model mice and patients, a proximity ligation assay (PLA) was performed by other trainees in the lab. This will be combined with my results to serve as a basis for a new publication on the project. The antibodies used are specific to SRC and PTP4A1 respectively. The assay makes use of the oligonucleotides linked to the secondary antibodies, which would hybridize to each other and serve as the primer and template for amplification only when the antigen proteins are interacting with each other. The fluorescent DNA probe will bind to any amplified template sequence and be visualized as fluorescent dots in confocal microscopy images.

Increased PLA signal between PTP4A1 and SRC was seen when NHDF were stimulated with TGFβ, which is consistent with previous results from the laboratory that PTP4A1 is induced by exogenous TGFβ in NHDF (Figure 11A). The known interaction between SRC and FAK was used as a positive control. The decrease in PLA signal in TGFβ-stimulated NHDF was significantly more marked upon PTP4A1 than PTP4A2 knockdown by ASO, which supports the hypothesis that SRC interacts more with PTP4A1 than PTP4A2 (Figure 11B). Lastly, the PLA signal was greatly enhanced in SScDF which show higher PTP4A1 expression levels compared to NHDF in the absence of TGFβ stimulation, consistent with the previous hypothesis that PTP4A1 levels are increased in SScDF due to their known autocrine TGFβ stimulation (Figure

11C). Thus, our data show a good correlation between PTP4A1 expression and the detected interaction between PTP4A1 and SRC in DF via PLA.

PLA was also performed on skin sections acquired from mice with bleomycin-induced fibrosis which were either WT or underwent conditional knockout of PTP4A1 in fibroblasts with Cre recombinase under the control of a Col1a1 promoter. Only when fibrosis was induced with bleomycin could a PLA signal between PTP4A1 and SRC be observed and the PLA signal was co-localized with αSMA which define pathogenic myofibroblasts. Selectively knocking out PTP4A1 in fibroblasts greatly decreased the PLA signal (Figure 12).

The PLA analysis was preliminarily extended to skin biopsy samples: biopsies from affected vs. non affected skin from one SSc patient were compared and these preliminary data also suggested that the interaction between PTP4A1 and SRC is more prominent in fibrotic tissue of SSc patients compared to their non-fibrotic tissue (Figure 13).

In conclusion, the PLA analysis successfully demonstrates a specific physical interaction of PTP4A1 and SRC in SSc dermal fibroblasts. Such specific interaction is triggered by TGFβ and correlates well with fibroblast activation by either exogenous TGFβ or imprinted alteration in autocrine TGFβ signaling in SSc fibroblasts, which cause overexpression of PTP4A1.

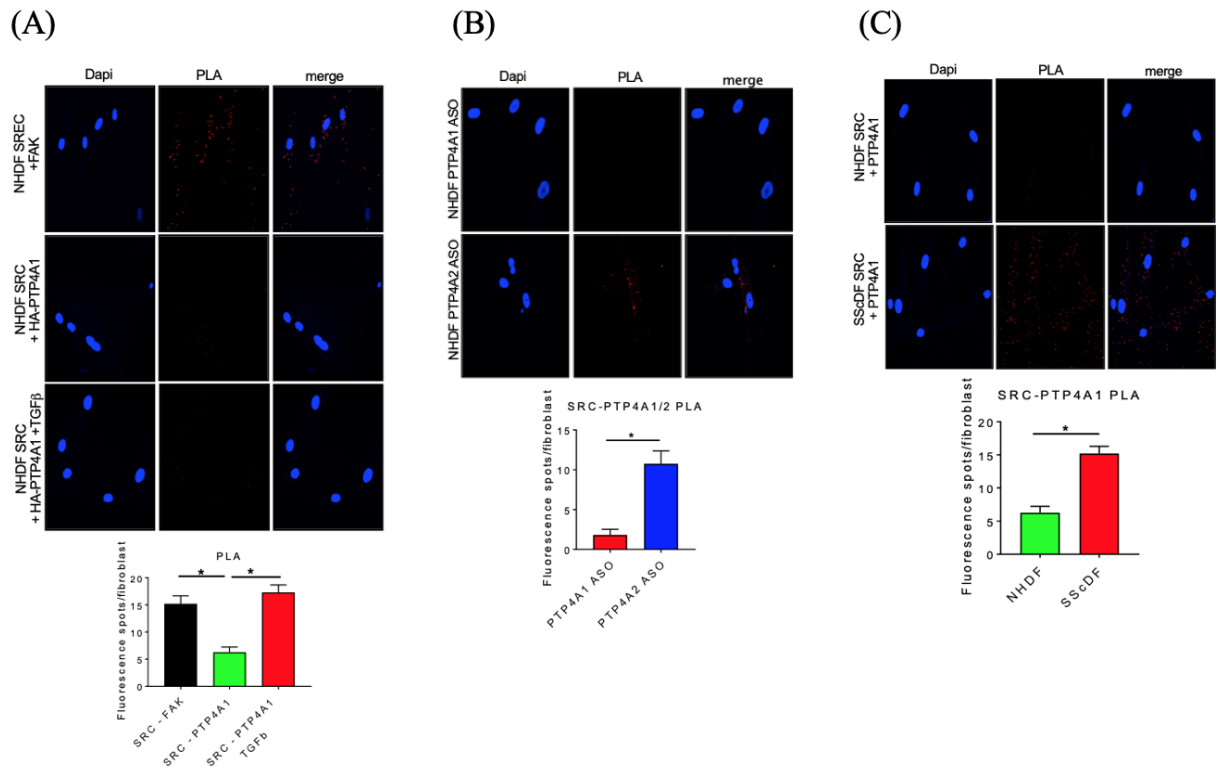

Figure 11. Proximity Ligation Assay (PLA) demonstrates a direct and specific interaction between PTP4A1 and SRC after TGFβ stimulation. (A) Representative immunostaining fluorescence microscopy images of PLA assays along with the quantification of fluorescence spots per cell demonstrate that the interaction between PTP4A1 and SRC was enhanced after TGFβ stimulation. (B) Representative immunostaining fluorescence microscopy images of PLA assays along with quantification of fluorescence spots per cell demonstrate that less interaction occurred when PTP4A1 is knocked down compared to PTP4A2. (C) Representative immunostaining fluorescence microscopy images of PLA assays along with quantification of fluorescence spots per cell demonstrate more interaction in SScDF. All quantification data in the figure are presented as mean ± SD (n = 3) and the statistical significance is analyzed with unpaired t-test with Welch's correction, *P<0.05.

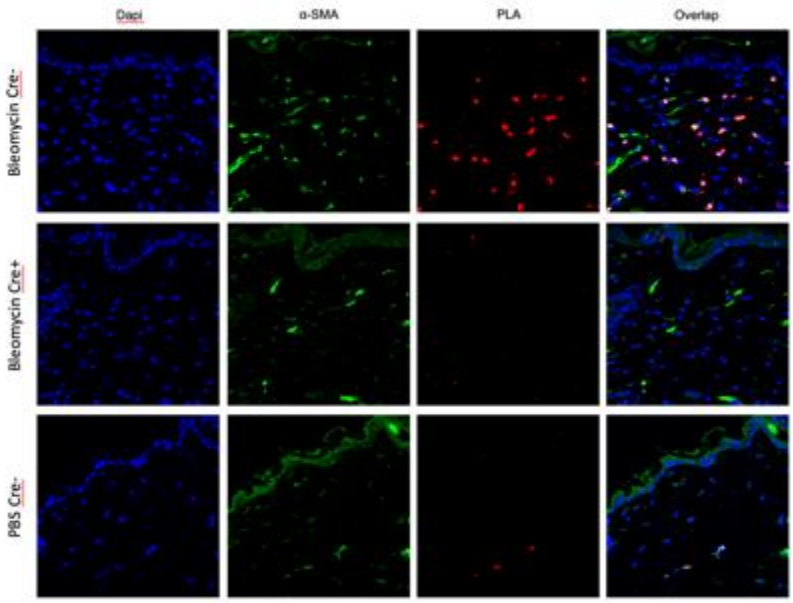

Figure 12. Proximity Ligation Assay (PLA) demonstrates the interaction between PTP4A1 and SRC and its co-localization with αSMA in the skin section of a bleomycin-induced fibrosis model. Representative immunostaining fluorescence microscopy images of PLA assays show that the interaction is greatly enhanced when the mice developed fibrosis due to bleomycin injection and that the PLA signal co-localizes with αSMA. Knocking down PTP4A1 in fibroblasts specifically greatly reduces both PLA (due to lack of PTP4A1) and αSMA (due to reduced fibrosis) signals.

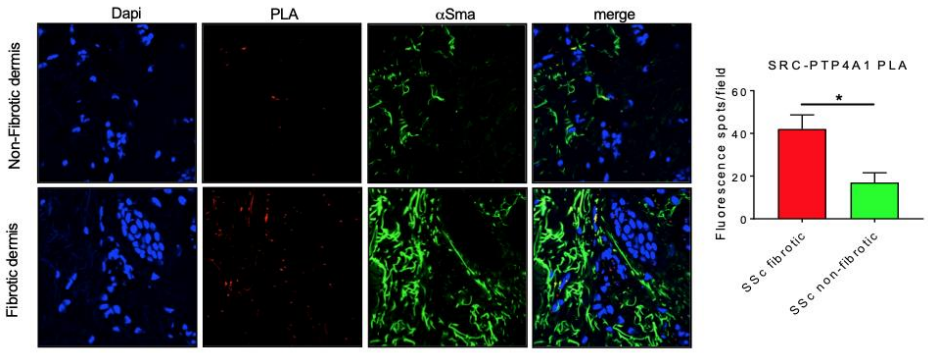

Figure 13. Preliminary proximity Ligation Assay (PLA) demonstrates enhanced interaction between PTP4A1 and SRC in fibrotic dermis of one SSc patient. Immunostaining fluorescence microscopy images of PLA assays along with the quantification of fluorescence spots per cell are shown. Data are presented as mean ± SD (n = 3) and the statistical significance is analyzed with unpaired t-test with Welch's correction, *P<0.05.

Discussion:

In this chapter, a PLA assay was performed on DF, fibrotic mouse tissues and skin specimens from one SSc patient by Cristiano and Denise, and it demonstrated interaction between PTP4A1 and SRC which correlated with TGFβ stimulation and TGFβ-induced fibrosis. The PLA assay significantly supports several conclusions we made from the previous study and the new biochemical assays. The interaction between PTP4A1 and SRC works downstream of TGFβ and mainly localized in fibroblasts displaying expression of αSMA. In SSc, there is not only excessive secretion of TGFβ by the activated immune system, but also hypersensitivity of fibroblasts towards TGFβ due to overexpression of TGFβ receptors and enhanced autocrine secretion of TGFβ by fibroblasts (38). Our current model is that the PTP4A1/Src interaction promotes TGFβ signaling thus overexpression of PTP4A1 through possibly epigenetic alteration induced by TGFβ during the early phases of the disease enables a positive feedback loop that amplifies pro-fibrotic signaling (1, 40). Albeit preliminary, the PLA data further support this hypothesis that the PTP4A1-SRC interaction is critical to the pathogenesis and progression of SSc and that the PTP4A1-SRC complex might serve as a good therapeutic target for the disease.

The PLA assay could be extended in the future to validate the factors that are found to be critical for the interaction in the in vitro co-precipitation assays. For example, NHDF could be incubated in oxidizing environment and analyzed with the PLA assay to assess whether the PTP4A1-SRC interaction is enhanced.

This chapter contains unpublished experiments coauthored with Cristiano Sacchetti, PhD and Denise Beckmann, PhD from the Bottini Lab. The thesis author was the primary author of this chapter.

REFERENCES

1. Sacchetti C, Bai Y, Stanford SM, Benedetto PD, Cipriani P, Santelli E, Piera-Velazquez S, Chernitskiy V, Kiosses BW, Ceponis A, Kaestner HK, Boin F, Jimenez AS, Giacomelli R, Zhang Z, Bottini N. PTP4A1 promotes TGFβ signaling and fibrosis in systemic sclerosis. *Nat Commun* 8, 1060 (2017).

2. Furst DE, Fernandes AW, Iorga SR, Greth W, Bancroft T. Epidemiology of systemic sclerosis in a large us managed care population. *J Rheumatol*. 39:784-786 (2012).

3. Allanore Y, Simms R, Distler O Trojanowska M, Pope J, Denton PC, Varga J. Systemic sclerosis. *Nat Rev Dis Primers* 1, 15002 (2015).

4. Denton CP, Khanna D. Systemic sclerosis. *Lancet* 390(10103):1685-1699 (2017).

5. Wirz EG, Jaeger VK, Allanore Y, Riemekasten G, Hachulla E, Distler O, Airo P, Carreira EP, Tikly M, Vettori S, Gurman BA, Damjanov N, Muller-Ladner U, Distler J, Li M, Hausermann P, Walker AU, EUSTAR coauthors. Incidence and predictors of cutaneous manifestations during the early course of systemic sclerosis: a 10-year longitudinal study from the EUSTAR database. *Annals of the Rheumatic Diseases* 75:1285-1292 (2016).

6. Sehriban D, Nathaniel D, Marie H, Tatibouet S, Fritzler JM, Baron M, Khalidi N, Canadian Scleroderma Research Group. Systemic Sclerosis Sine Scleroderma: A Multicenter Study of 1417 Subjects. *The Journal of Rheumatology* 41(11) 2179-2185 (2014).

7. Korman B. Evolving insights into the cellular and molecular pathogenesis of fibrosis in systemic sclerosis. *Transl Res* 209:77-89 (2019).

8. Trojanowska M. Cellular and molecular aspects of vascular dysfunction in systemic sclerosis. *Nat Rev Rheumatol* 6, 453–460 (2010).

9. Chizzolini C, Parel Y, Scheja A, Dayer J. Polarized subsets of human T-helper cells induce distinct patterns of chemokine production by normal and systemic sclerosis dermal fibroblasts. *Arthritis Res Ther* 8, R10 (2006).

10. Varga J, Pasche B. Transforming growth factor β as a therapeutic target in systemic sclerosis. *Nat Rev Rheumatol* 5, 200–206 (2009).

11. Distler O, Highland KB, Gahlemann M, Azuma A, Fischer A, Mayes DM, Raghu G, Sauter W, Girard M, Alves M, Clerisme-Beaty E, Stowasser S, Tetzlaff K, Kuwana M, Maher MT, SENSCIS Trial Investigators. Nintedanib for Systemic Sclerosis-Associated Interstitial Lung Disease. *N Engl J Med* 380(26):2518-2528 (2019).

12. Alonso A, Sasin J, Bottini N, Friedberg I, Friedberg I, Osterman A, Godzik A, Hunter T,

Dixon J, Mustelin T. Protein tyrosine phosphatases in the human genome. *Cell* 117(6):699-711 (2004).

13. Stephens BJ, Han H, Gokhale V, Von Hoff DD. PRL phosphatases as potential molecular targets in cancer. *Mol Cancer Ther* 4(11):1653-1661 (2005).

14. He RJ, Yu ZH, Zhang RY, Zhang ZY. Protein tyrosine phosphatases as potential therapeutic targets. *Acta Pharmacol Sin* 35(10):1227-1246 (2014).

15. Zeng Q, Si X, Horstmann H, Xu Y, Hong W, Pallen CJ. Prenylation-dependent association of protein-tyrosine phosphatases PRL-1, -2, and -3 with the plasma membrane and the early endosome. *J Biol Chem* 275(28):21444-21452 (2000).

16. Jeong DG, Kim SJ, Kim JH, Son JH, Park MR, Lim SM, Yoon T, Ryu SE. Trimeric structure of PRL-1 phosphatase reveals an active enzyme conformation and regulation mechanisms. *J Mol Biol* 345(2):401-413 (2005).

17. Sun J, Wang W, Yang H, Liu S, Liang F, Fedorov AA, Almo CS, Zhang Z. Structure and biochemical properties of PRL-1, a phosphatase implicated in cell growth, differentiation, and tumor invasion. *Biochemistry* 44(36):12009-12021 (2005).

18. Peters CS, Liang X, Li S, Kannan S, Peng Y, Taub R, Diamond RH. ATF-7, a novel bZIP protein, interacts with the PRL-1 protein-tyrosine phosphatase. *J Biol Chem* 276(17):13718-13726 (2001).

19. Giménez-Mascarell P, Oyenarte I, Hardy S, Breiderhoff T, Stuiver M, Kostantin E, Diercks T, Pey LA, Ereno-Orbea J, Martinez-Chantar LM, Khalaf-Nazzal R, Claverie-Martin F, Muller D, Tremblay LM, Martinez-Cruz AL. Structural Basis of the Oncogenic Interaction of Phosphatase PRL-1 with the Magnesium Transporter CNNM2. *J Biol Chem* 292(3):786-801 (2017).

20. Ishii T, Funato Y, Miki H. Thioredoxin-related protein 32 (TRP32) specifically reduces oxidized phosphatase of regenerating liver (PRL). *J Biol Chem* 288(10):7263-7270 (2013).

21. Hardy S, Kostantin E, Hatzihristidis T, Zolotarov Y, Uetani N, Tremblay ML. Physiological and oncogenic roles of the PRL phosphatases. *FEBS J* 285(21):3886-3908 (2018).

22. Jiao Y, Ye DZ, Li Z, Teta-Bissett M, Peng Y, Taub R, Greenbaum EL, Kaestner HK. Protein tyrosine phosphatase of liver regeneration-1 is required for normal timing of cell cycle progression during liver regeneration. *Am J Physiol Gastrointest Liver Physiol* 308(2):G85-G91 (2015).

23. Urwyler O, Izadifar A, Vandenbogaerde S, Sachse S, Misbaer A, Schmucker D. Branch-restricted localization of phosphatase Prl-1 specifies axonal synaptogenesis domains.

Science 364(6439):eaau9952 (2019).

24. Roskoski R Jr. SRC protein-tyrosine kinase structure, mechanism, and small molecule inhibitors. *Pharmacol Res*. 94:9-25 (2015).

25. Xu W, Doshi A, Lei M, Eck MJ, Harrison SC. Crystal structures of c-SRC reveal features of its autoinhibitory mechanism. *Mol Cell*. 3(5):629-638 (1999).

26. Seeliger MA, Young M, Henderson MN, Pellicena P, King SD, Falick MA, Kuriyan J. High yield bacterial expression of active c-Abl and c-SRC tyrosine kinases. *Protein Sci* 14(12):3135-3139 (2005).

27. Murrell DF. A radical proposal for the pathogenesis of scleroderma. *J Am Acad Dermatol*.28(1):78-85 (1993).

28. Vona R, Giovannetti A, Gambardella L, Malorni W, Pietraforte D, Straface E. Oxidative stress in the pathogenesis of systemic scleroderma: An overview. *J Cell Mol Med*. 22(7):3308-3314 (2018).

29. Gulerez I, Funato Y, Wu H, Yang M, Kozlov G, Miki H, Gehring K. Phosphocysteine in the PRL-CNNM pathway mediates magnesium homeostasis. *EMBO Rep*. 17(12):1890-1900 (2016).

30. Skinner AL, Vartia AA, Williams TD, Laurence JS. Enzyme activity of phosphatase of regenerating liver is controlled by the redox environment and its C-terminal residues. *Biochemistry*. 48(20):4262-4272 (2009).

31. Snyder MA, Bishop JM, McGrath JP, Levinson AD. A mutation at the ATP-binding site of pp60v-SRC abolishes kinase activity, transformation, and tumorigenicity. *Mol Cell Biol*. 5(7):1772-1779 (1985).

32. Kamps MP, Sefton BM. Neither arginine nor histidine can carry out the function of lysine-295 in the ATP-binding site of p60SRC. *Mol Cell Biol*. 6(3):751-757 (1986).

33. Lee JO, Jeong D, Kim MY, Cho JY. ATP-Binding Pocket-Targeted Suppression of SRC and Syk by Luteolin Contributes to Its Anti-Inflammatory Action. *Mediators Inflamm*. 2015:967053 (2015).

34. Harris KF, Shoji I, Cooper EM, Kumar S, Oda H, Howley PM. Ubiquitin-mediated degradation of active SRC tyrosine kinase. *Proc Natl Acad Sci*. 96(24):13738-13743 (1999).

35. Kmiecik TE, Shalloway D. Activation and suppression of pp60c-SRC transforming ability by mutation of its primary sites of tyrosine phosphorylation. *Cell*. 49(1):65-73 (1987).

36. Roskoski R Jr. Src kinase regulation by phosphorylation and dephosphorylation. *Biochem Biophys Res Commun*. 331(1):1-14 (2005).

37. Skinner AL, Laurence JS. 1H, 15N, 13C resonance assignments of the reduced and active form of human Protein Tyrosine Phosphatase, PRL-1. *Biomol NMR Assign*. 3(1):61-65 (2009).

38. Kawakami T, Ihn H, Xu W, Smith E, LeRoy C, Trojanowska M. Increased expression of TGF-beta receptors by scleroderma fibroblasts: evidence for contribution of autocrine TGF-beta signaling to scleroderma phenotype. *J. Invest. Dermatol*. 110, 47–51 (1998).

39. Brown MT, Cooper JA. Regulation, substrates and functions of SRC. *Biochim Biophys Acta*. 1287(2-3):121-149 (1996).

40. Altorok N, Tsou PS, Coit P, Khanna D, Sawalha AH. Genome-wide DNA methylation analysis in dermal fibroblasts from patients with diffuse and limited systemic sclerosis reveals common and subset-specific DNA methylation aberrancies. *Ann Rheum Dis*. 74(8):1612-1620 (2015).